Article

Signal Transformations for Analysis of Supraharmonic EMI Caused by Switched-Mode Power Supplies

Leonardo Sandrolini [1,*] **and Andrea Mariscotti** [2]

1   Department of Electrical, Electronic and Information Engineering (DEI), University of Bologna,
    40126 Bologna, Italy
2   Department of Electrical, Electronics and Telecommunication Engineering and Naval Architecture (DITEN),
    University of Genova, 16145 Genova, Italy; andrea.mariscotti@unige.it
*   Correspondence: leonardo.sandrolini@unibo.it; Tel.: +39-051-2093-484

check for
updates

Abstract: Switched-Mode Power Supplies (SMPSs) are a relevant source of conducted emissions, in particular in the frequency interval of supraharmonics, between 2 kHz and 150 kHz. When using sampled data for assessment of compliance, methods other than Fourier analysis should be considered for better frequency resolution, compact signal energy decomposition and a shorter time support. This work investigates the application of the Wavelet Packet Transform (WPT) and the Empirical Mode Decomposition (EMD) to measured recordings of SMPS conducted emissions, featuring steep impulses and damped oscillations. The comparison shows a general accuracy of the amplitude estimate within the variability of data themselves, with very good performance of WPT in tracking on stationary components in the low frequency range at some kHz. WPT performance however may vary appreciably depending on the selected mother wavelet for which some examples are given. EMD and its Ensemble EMD implementation show a fairly good accuracy in representing the original signal with a very limited number of base functions with the capability of exploiting a filtering effect on the low-frequency components of the signal.

Keywords: electromagnetic compatibility; conducted emissions; Discrete Wavelet Transform; electromagnetic interference; Empirical Mode Decomposition; harmonics; Switched-Mode Power Supplies; transients; Wavelet Packet Transform

1. Introduction

The widespread use of Switched-Mode Power Supplies (SMPSs) can be justified with flexibility, portability and better efficiency, including superior voltage regulation at the dc load. SMPSs feature various types of power electronic converters topologies, with conducted emissions that need to be assessed over a wide frequency range [1]. Conducted emissions caused by the switching process, in fact, originate from switching fundamentals of some tens of kHz and spread in the hundreds kHz and MHz ranges, well above the "classical" interval of harmonic and interharmonic penetration studies, limited in general to some kHz for 50–60 Hz systems. In the last ten years, attention has been extended to frequency intervals below 150 kHz [2–9], in general not currently regulated by electromagnetic compatibility (EMC) standards, focusing on the so-called "supraharmonics". Some standards [10–14] deal with the 2–150 kHz interval, but do not cover explicitly SMPSs and other similar switching converters, thus taking into account the characteristics of the related signals. The approach of EMC standards to the quantification of conducted emissions is quite similar above and below 150 kHz: resolution bandwidth of 9 kHz and frequency sweep by a spectrum analyzer or EMI receiver is the reference approach. However, the use of time-domain sampling is a valid alternative for the many data acquisition boards and digital sampling oscilloscopes available, for the possibility of inspecting the

"real" waveform when cross-checking the final results (especially in case of noncompliance) and the possibility of changing and tuning the post-processing methods.

The most popular of these methods is the spectrum calculation by Fourier transform (a Discrete Fourier Transform (DFT) or a Short-Time Fourier Transform (STFT), tracking Fourier spectrum versus time): it is a well-known technique that can be mastered after some practice, but may in reality lead to some disappointment, especially in the case of transient signals with a short time support [15], as it briefly pointed out in Section 2. Alternative methods better suited to handle signals characterized by transients may be considered: wavelets with the Wavelet Packet Transform (WPT) [16–22] and the Empirical Mode Decomposition (EMD), in the Ensemble EMD (EEMD) implementation [23–26] (to avoid the EMD shortcomings, as shown in Section 2). Although they have both been extensively described in the literature and the former applied often to Power Quality analysis, the considered problem is peculiar in two aspects:

- The investigated methods must provide accurate results in terms of amplitude of the signal components that may be compared to existing or future emission limits, in order to assess compliance and related margins. Several wavelet applications do not discuss the amplitude accuracy in the presence of both narrowband and broadband components, as well as of significant variability of the instantaneous frequency.
- They must support the analysis of the signal and of the control measures necessary in the case of noncompliance, with clear relationship with the internal sources and switching mechanisms, as well as also being easily interpretable, at least for the most relevant components critical for compliance to limits.

Modern controllers for switching converters adopt smart modulation techniques to improve efficiency, reduce voltage stress on components and reduce EMI. They are able to rapidly switch between different modulation patterns, each optimized for a range of operations and possibly with different spectral signatures: this opens the door to potential non-stationarity of the signal and the need to adopt short time windows, unsuitable for a Fourier-based approach.

Traditional EMC techniques based on frequency sweep have fallen behind the technological development in some sectors, such as power transfer and conversion [27], as well as in the presence of significant transients as the first source of emissions [28]. They would benefit from time–frequency analysis methods that are computationally attractive and preserve the accuracy necessary for the assessment of compliance. The focus is on amplitude accuracy, with the frequency estimate used only to locate suitable limit values and track component behavior. The definition of a reference case for comparison is particularly challenging, as discussed in Section 3.

This work describes the setup and measurement methods in Section 2. Then, after a synthetic description in Section 3 of the WPT and EMD transforms (with a comparison between EMD and EEMD), results are compared and discussed in Section 4.

2. Measurement Setup and Signal Transformations

2.1. Measurement Setup

The signals considered in this work are the conducted emissions of SMPSs connected to the AC mains through a Line Impedance Stabilization Network (LISN). The output of the LISN is fed to an 8-bit DSO with a sampling rate of 10 MSa/s, to keep records to a manageable size for later post-processing. Frequency domain sweeps can be carried out as well by means of an EMI receiver, to use as reference in case of need. The scheme of the setup is shown in Figure 1.
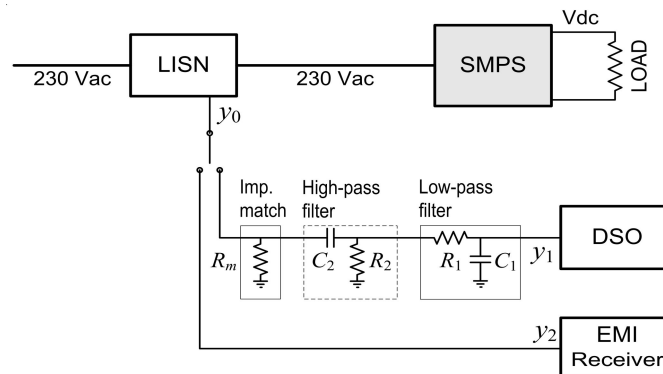
Figure 1. Scheme of the experimental setup: SMPS under test and its dc variable load, LISN (Line Impedance Stabilization Network), 50 Ω impedance matching, high-pass filter (1 kHz cutoff) and low-pass filter (2 MHz cutoff), Digital Storage Oscilloscope (DSO) and EMI Receiver.

An anti-aliasing low-pass filter with a cutoff frequency of 2 MHz is used to feed the DSO: the resistor R_2 is 5 kΩ and the capacitance C_2 is the internal input capacitance of the DSO, equal to 15 pF with good accuracy. A high-pass filter with a cutoff frequency of 1 kHz is also included for additional attenuation of the fundamental and the 100 Hz ripple component possibly leaking through the LISN: the resistor R_1 = 1.5 kΩ is large enough to be neglected in parallel to the impedance-matching 50 Ω resistor R_m, giving a neat 100 nF for C_1 to get the desired 1 kHz cutoff.

The tested SMPSs are all AC/DC low-voltage switching converters with a 5 V or 12 V nominal dc output and a power level in the range of some tens of W. This allowed the use of a 16 A LISN and no major issues of heating and high-voltage hazards; it is not likewise a limiting factor, since it is expected that smaller converters will show the most rapid switching transients. As a matter of fact, the observed switching frequency values are in the range of some tens of kHz, in line with the dynamics of controllers and MOS transistors available about ten years ago.

The switching byproducts responsible for the conducted emissions are superimposed to the mains sinusoidal voltage, located at its zero crossings. The signal y_1 at the DSO input (qualitatively similar to the signal y_0 as provided at the LISN output) is an intermittent waveform, deprived of the 50 Hz mains voltage component and of its low-order harmonics, also to improve the dynamic range. The zero-mean high-pass filtered signal is characterized by steep transients and rapid oscillations, as shown in Figure 2. The instantaneous frequency of oscillations is in the order of 20–30 kHz and is in relation to the internal switching frequency; the repetition rate is 100 Hz, twice the mains frequency.
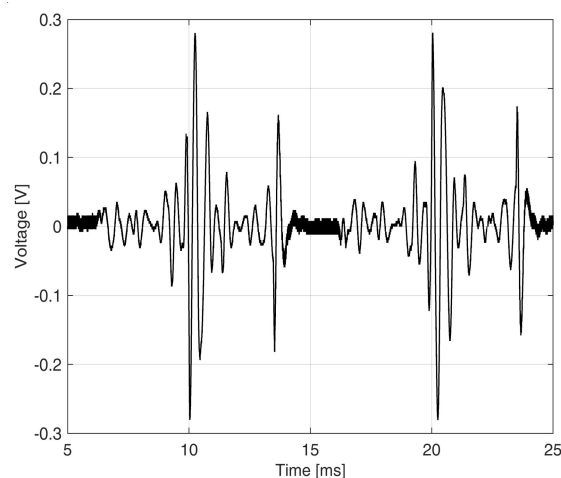
Figure 2. Typical time-domain waveform of an SMPS at the high-pass filtered LISN output measured as DSO input signal y_1.

2.2. Use of the Discrete Fourier Transform (DFT)

The Fourier-based analysis, for simplicity gathered under the abbreviation DFT, is assumed well known and is not repeated. As seen, the signal is characterized by bursts with oscillations at low and high frequency of limited duration. The use of DFT applied to this kind of intermittent rapidly varying signals has the following drawbacks:

- The signal portion to analyze has a short duration, which contrasts to the desirable or required frequency resolution. The IEC 61000-4-7 standard [29] indicates an observation time of 200 ms that is clearly inadequate (equivalent to 5 Hz resolution, suitable for low frequency harmonics, but not for phenomena at higher frequency with fast dynamics, as in the present case). The EN 55065-1 [14] and in general EMC standards for conducted emissions below 150 kHz require a 200 Hz resolution bandwidth. A more suitable approach has been proposed in the IEC 61000-4-30 [13], defining a frequency resolution of 2 kHz, which goes in the direction of tracking signals with fast dynamics, as in the present case.
- To avoid spectral leakage, the signal should be cut in the zero-valued short intervals between pulses, implying a resolution frequency of about 100 Hz. Other window intervals will suffer from spectral leakage, only partly attenuated by the use of tapering windows.
- Using a long window interval has the drawback of averaging the contribution of the contained signal components, largely reducing the estimated amplitude of the peak located at the center.
- Using a short window interval reduces the frequency resolution and worsens the spectral representation and the estimate of the amplitude, this time caused by the short-range spectral leakage (or "picket fence effect"), if no additional post processing is used.

For all the reasons above and as justified in the Introduction, alternative signal transformations should be investigated for applicability to the present case, providing spectral representations in a domain (or combination of domains, e.g., time and frequency) that can still be interpreted and used to evaluate the degree of compliance, as for conducted emissions in the aforesaid 2–150 kHz interval. Wavelets have been extensively applied for accurate PQ analysis in the harmonic low-frequency range [1,16,18–21], as effective alternative method for compliance to the IEC 61000-4-30 processing requirement and for detection of transient PQ phenomena (e.g., voltage sags, overvoltages, etc.) [17], the latter without the analysis of the accuracy of the parameters estimate. EMD and EEMD find their application in the analysis of seismic data, vibrations, speech signals and medical data [23–25], but lack a clear quantification of component amplitude to support comparison with limits and susceptibility criteria, defined in the frequency domain. Rather their typical application is more oriented to the detection and identification of signal features and components hidden by noise and signal compression.

2.3. Wavelet Packet Transform (WPT)

Oppositely to the DFT with its stationary sinusoidal kernel, wavelet analysis relies on short-duration oscillating waveforms that have zero mean and decay rapidly to zero at both ends [16]. Dilation and shifting of kernel waveforms allow adapting it for variable time and frequency resolution. Since its first inception, wavelets have been proposed in both wavelet function and multistage filter bank implementations. The filter bank was built using low-pass (LP) and high-pass (HP) complementary filters (for reference, they can be created as "quadrature mirror filters") [16,18]. The first implementation (Discrete Wavelet Transform (DWT)) applied recursively the LP and HP filters of the successive stage only to the LP output of the previous stage, and so on. The Wavelet Packet Transform (WPT) uses then a symmetrical structure, applying the decomposition to both LP and HP outputs, as shown in Figure 3, which allows a linear, rather than logarithmic, apportionment of the frequency axis, and thus a linear decomposition of the signal spectrum. This is inline with the 2 kHz group representation uniformly spread over the frequency axis suggested by the EN 61000-4-30 [13]. At each stage, the outputs of the LP and HP filters are named "approximation" and "detail", respectively.
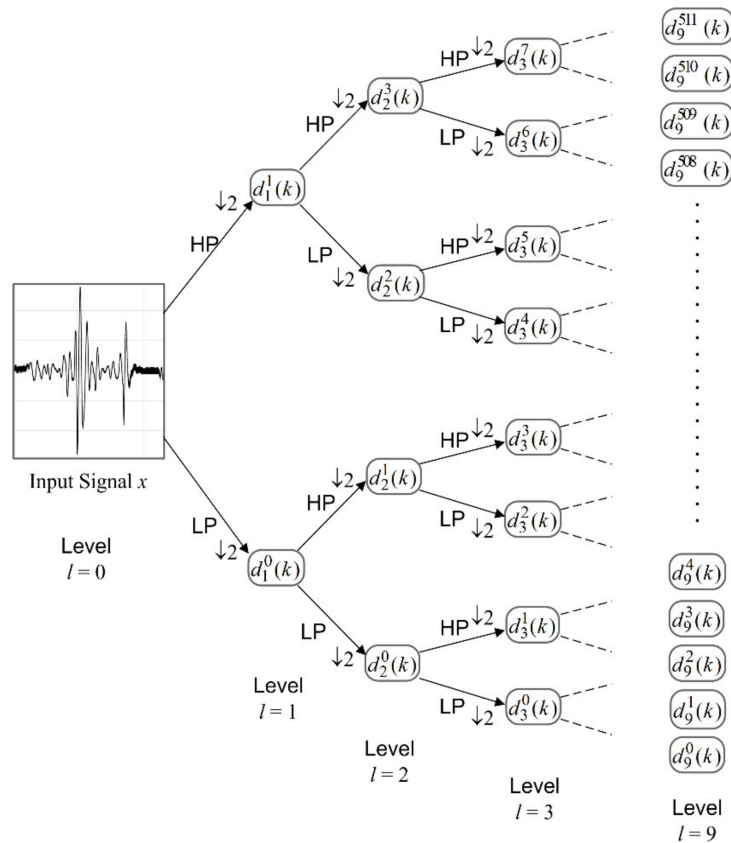
Figure 3. WPT (Wavelet Packet Transform) tree structure, indicating levels, ordinal indices at each level and terminal nodes. The down arrow "↓n" indicates a down sampling (or decimation) by a factor of n (in our case, n = 2).

The output of the WPT decomposition is used for a compact spectrum estimate focused on the determination of three elements: the amplitude of the component, its location on the frequency axis and its location on the time axis (or duration). The STFT addresses this third point by assigning a window length and the amount of overlap between successive windows sliding over the signal along the time axis.

The WPT spectrum estimate is built on the "details" of the terminal nodes, which are in a number $N = 2^L$, where L is the number of chosen levels. Details are denoted as $d_l^p(k)$, where l indicates the level ($l = 0, 1, \ldots L$, level 0 being the original signal x), p is the position along the row of nodes in the tree at the same level ($p = 0, 1, \ldots 2^l$) and k is a "time" index (the position along the sequence of data samples). Each detail in fact apportions the original signal of length M over the N nodes at a given level with data sequences of length M/N; the lower in the tree, the higher the level l and the number of nodes ($N_l = 2^l$), and the shorter the length of each sequence $K = M/2^l$. Each data sequence contained by a detail (for ease of understanding, we consider the last and deeper level, i.e., the terminal nodes) is a sub-band representation of the original signal: the bandwidth, or frequency resolution, Δf is derived from the original sampling f_s as $\Delta f = f_s/2^{L+1}$, and in general $\Delta f_l = f_s/2^{l+1}$. In our case with a downsampled version of the raw data using $f_s = 1$ MSa/s and $L = 9$, we obtain $\Delta f = 976$ Hz, which matches the selected RBW for the EMI receiver data used for comparison in Section 3.

To the aim of the quantitative assessment of the accuracy of WPT spectrum estimate, the amplitude of the components of the spectral representation must be derived: the Matlab function wpspectrum( ) gives such time–frequency representation, where time and frequency resolutions Δt and Δf are determined by the selected number of levels L and the original sampling f_s.

The problem is to understand the unity of measure and the meaning of the spectrum values (pixels, or tiles) in terms of the original quantities; in other words, WPT spectrum extraction needs to be "calibrated" in order to be used as an EMI assessment tool.

Given the details as sub-banded data sequences, the calculation of the total rms value gives straightforwardly a measure of the power contained in each sub-band *p* (the notation $l = L$ in (1) indicates that the expression is general for whatever *l*, but we select in the following $l = L$, so that the terminal nodes give the desired frequency resolution).

$$\widetilde{x}_{p,l=L} = \sqrt{\frac{\sum\limits_{k} (d^p_{l=L}(k))^2}{N_{l=L}}} \tag{1}$$

Of course, rms values from adjacent sub-sequences may be aggregated with a concept of overall rms in a wider band, made of the composition of each respective Δf^p_l (the sub-band of order *p* at the level *l*). Being rms values interpreted in a power perspective, such aggregation is performed by rms summation over the sub-sequences $d^p_L(k)$ with *p* in the selected α set (written as p_α).

$$\widetilde{x}_{[p_\alpha],L} = \sqrt{\frac{\sum\limits_{\alpha} \sum\limits_{k} (d^{p_\alpha}_L(k))^2}{N_L}} \tag{2}$$

To exemplify, to make an approximately 2 kHz representation from the $\Delta f = 976$ Hz representation, two adjacent sub-bands must be aggregated, discarding the first one that contains the dc component. Thus, the *p* indices would start from 1 and go in pairs: (2,3), (4,5), (6,7), etc. A bandwidth of approximately 3 kHz is obtained by grouping with a ratio of 3, so (2,3,4), (5,6,7), etc.

2.4. Empirical Mode Decomposition (EMD) and Ensemble Empirical Mode Decomposition (EEMD)

The Empirical Mode Decomposition (EMD) was proposed for attractive characteristics: the transformation is based on simple operations (and should be relatively light computationally), its results can be clearly interpreted and it is robust, thus there are no wide or uncontrolled variations of the results for small changes of the parameters.

The EMD was developed to prepare the data to which the Hilbert Transform (HT) could be applied; the combination of EMD and HT is the Hilbert-Huang Transform (HHT), which provides a powerful tool for nonlinear and nonstationary signal processing. The signal is decomposed adaptively into a finite (often small) number of the so-called Intrinsic Mode Functions (IMFs), not known a priori (differently than in the Fourier or Wavelet analysis), which represent the oscillation modes embedded in the data. With the HT, the IMFs yield instantaneous frequencies as functions of time. Each IMF satisfies the following two conditions:

- In the whole dataset, the number of extrema and the number of zero crossings is either equal or differ at least by one.
- At any point, the mean value of the envelope defined by local maxima and local minima is zero.

The iterative process of extraction of the IMFs through the EMD method is called the sifting process. The first IMF contains the highest oscillation frequency in the signal. The difference between the original signal and the first IMF is called a residue. The residue is then considered as new data to decompose and the sifting process is applied to it; the same definition thus applies to the difference between the previous residue and the last IMF at later stages. The sifting process must be repeated until the extracted signal (the candidate IMF) satisfies the IMF definition or the predefined maximum number of iterations is exceeded. The number of extrema decreases as the decomposition proceeds, and the sifting process ends when the residue becomes a monotonic function or a function with only one extremum from which no further IMF can be extracted [23] (in other words, no oscillations are

contained in the residue). At the end of the decomposition, we have N IMF functions and one residue, and the original signal $x(t)$ can be reconstructed as

$$x(t) = \sum_{i=1}^{N} c_i(t) + r(t) \tag{3}$$

where c_1 and c_N are the highest and lowest frequency IMFs, respectively, and $r(t)$ is the residue. Besides the harmonic content, IMFs are characterized by different amplitudes. The original signal may then be fairly approximated by using only a limited set of the IMFs, i.e., those with the largest amplitudes only.

The major drawback of the EMD method is mode mixing, for which the EEMD method was introduced [26]. Mode mixing means that different modes of oscillations coexist in the same IMF. EEMD (Ensemble EMD) consists in adding white noise to the original signal. This procedure is run for a number of times, thus an ensemble of datasets with different added white noise is generated. The new obtained data are then decomposed into IMFs with the sifting procedure. Being the added noise different in each run, the IMFs of the various runs are uncorrelated. Averaging the IMFs eliminates the added noise and yields then the final result. The truth IMF, $c_j(t)$, defined by EEMD is then obtained for an ensemble number approaching infinity:

$$c_j(t) = \lim_{N \to \infty} \sum_{k=1}^{N} c_{jk}(t) \tag{4}$$

where

$$c_{jk}(t) = c_j(t) + r_{jk}(t) \tag{5}$$

is the kth trial of the jth IMF in the noise added signal, being $r_{jk}(t)$ the contribution from the added white noise of the kth trial to the jth IMF. To minimize the difference between the truth IMF $c_j(t)$ and the IMF $c_j(t)$ obtained with N trials, N must be large, as for the well-known statistical rule the difference between the truth and the result of the ensemble for a finite number of elements of the ensemble decreases as $1/\sqrt{N}$.

EEMD represents a major improvement to EMD as it eliminates mode mixing; however, the major drawback is that the result of EEMD does not strictly satisfy the definition of IMF, as the sum of IMFs is not necessarily an IMF. A possible solution to this problem is to apply EMD to the IMFs produced by EEMD.

3. Results

3.1. Introduction and Reference Case

Regarding the accuracy of the estimated amplitude, it is difficult to establish a reference case for this kind of signals. In other words, what is the real amplitude of the spectrum components of the signal?

The STFT gives a first indication, although the amplitude is highly variable, as a function of the frequency resolution, its implicit averaging and the amount of spectral leakage depending on the characteristics of the adopted tapering window.

It may be objected that an EMI receiver scan returns the reference spectrum, since after all it is the reference method adopted by EMC standards, against which we check the compliance of emissions. The "EMC" resolution bandwidth (RBW) values of 200 Hz and 9 kHz used, respectively, below and above 150 kHz have been considered as a starting point, assessing the variability of the measured spectrum by changing RBW from 200 Hz to 1 kHz, 2 kHz, 3 kHz and 5 kHz, looking for a compromise between a neat frequency resolution and an accurate amplitude estimate. The results are reported in Figure 4 showing a progressive increase of the noise floor (as expected), a substantially stable amplitude

of the switching peaks at 43.3 kHz and 87 kHz and above, and a variable estimated amplitude for the low-frequency nonstationary components (with a behavior similar to that of background noise). The result with 1 kHz RBW is retained for further analysis as a good compromise, also in view of the necessary time resolution settings in STFT and WPT.
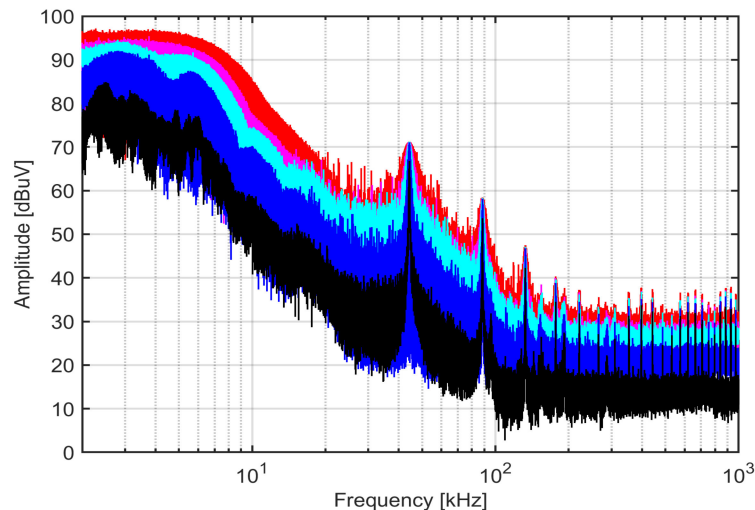
Figure 4. EMI receiver spectra with variable RBW (200 Hz, black; 1 kHz, blue; 2 kHz, light blue; 3 kHz, magenta; 5 kHz, red) for a SMPS featuring fixed switching frequency (type Black at 90% of rated power).

A slower narrow-RBW scan should be used instead (e.g., with RBW = 10 Hz or 30 Hz): the dynamic range will be maximized and, using the "max hold" setting at each frequency bin (or step), it is ensured that the repeatability of the measurement is also maximized. However, such setting is quite far from those used for measurement of emissions and the necessary scan time is extremely long (about 8 h), yielding issues of long-term stability of the setup.

3.2. Performance of WPT

3.2.1. Basic Time and Frequency Resolution Performance of WPT

The time resolution of both WPT spectra in Figure 5b,c is superior to that of STFT tracking the signal with 500 μs and 125 μs steps, respectively; considering the visible signal dynamics and what is offered by alternative approaches (such as a narrowband DFT or a real-time spectrum analyzer), a time step in this range is more than adequate. Correspondingly, the frequency resolution also varies by a factor of 4 in the opposite direction: when using 976 Hz in Figure 5b, the low-frequency portion of the spectrum is enriched with the details between the second and the sixth bin, which hold alternatively the maximum of the spectrum around $t = 5$ ms; this is evident from the asymmetry of the half-cycles of the oscillatory spike in the center of the waveform of Figure 5a. The comparison of the estimated amplitudes for the two spectra with different frequency and time resolution indicates that a finer time resolution gives slightly larger amplitudes (Figure 5c), avoiding the averaging implicit in a larger time interval. This behavior is common with the DFT and is hardly predictable quantitatively, as it depends on the characteristics of the signal components (narrowband/broadband and steady/transient). The average of four adjacent time bins in Figure 5c gives approximately the value of one bin of Figure 5b (within 1 dB). Nonetheless, the maximum value can differ by up to 3.4 dB, as occurring in the first frequency bin at 5 ms; this represents then the maximum absolute error between the two spectral representations.

(**a**)

(**b**)

(**c**)
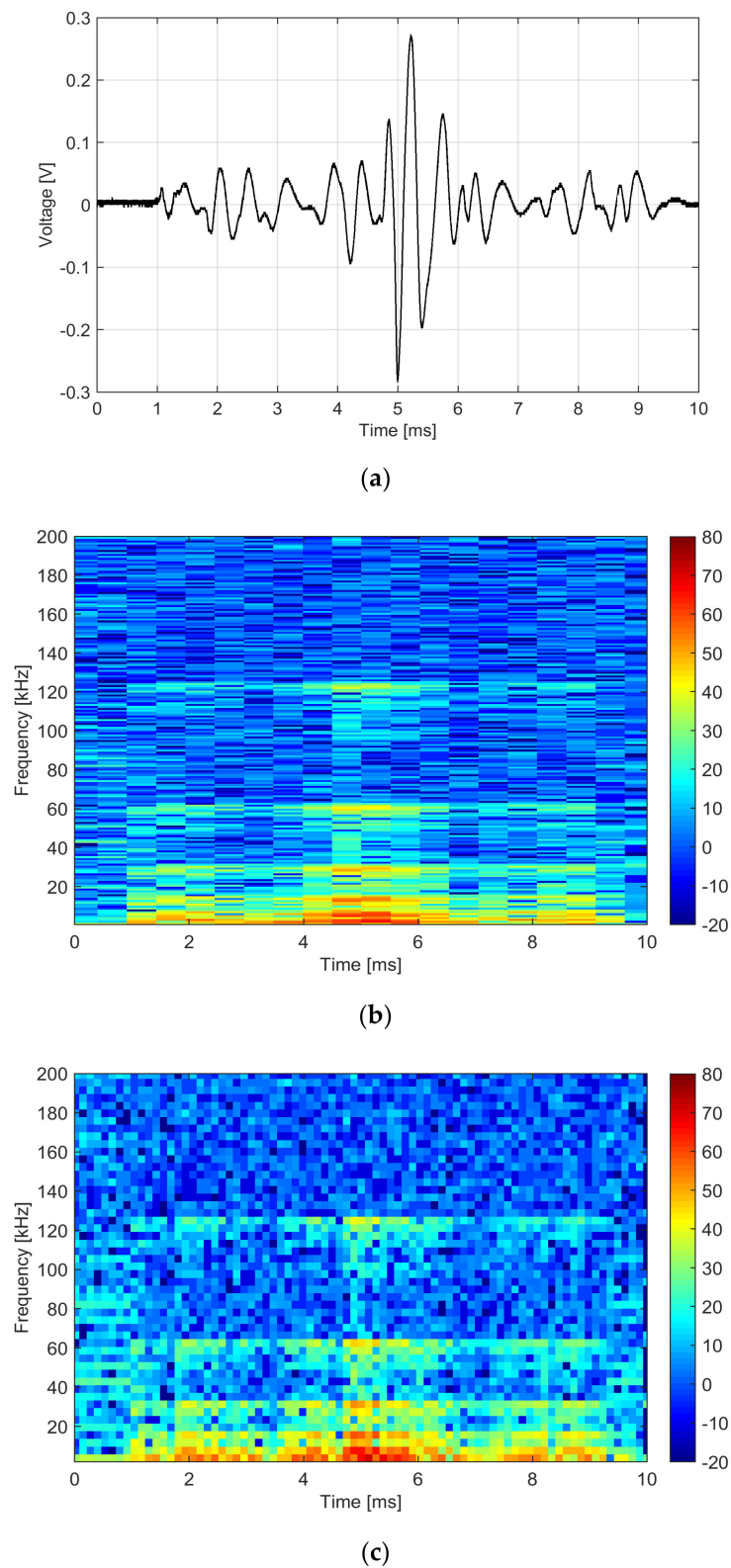
Figure 5. WPT spectrum in dBμV/Hz (normalized by frequency resolution). An example of change of dilation in time and frequency by a factor of 4 with *symlet1* wavelet: (**a**) signal waveform (10 MSa/s); (**b**) *symlet1* with $L = 9$ levels and a downsampling of $q = 10$; and (**c**) *symlet1* with $L = 8$ levels and $q = 5$. SMPS type Black at 25% of rated power.

The case of two different wavelets is shown in Figure 6, applied to the signal using the same scaling: the amplitude estimates are quite similar, with the *bior1.3* in Figure 6b, showing slightly smoother amplitude profile than the *symlet1*. Quantitatively, the average difference for the bins with the largest amplitude (those in Figure 6 with amplitude above 50 dB) is only 1.3 dB; the peaks, which are the most relevant for compliance to limits, are reproduced quite reliably with almost identical values (average difference of less than 0.25 dB). Thus, at least for the considered case, the choice of wavelets with "similar" characteristics and of suitable order for the observed time support gives repeatable results, although it represents a source of systematic error and the contribution to the uncertainty of the estimate of spectrum amplitude is not negligible (0.25 dB on average for the considered case).

(**a**)

(**b**)
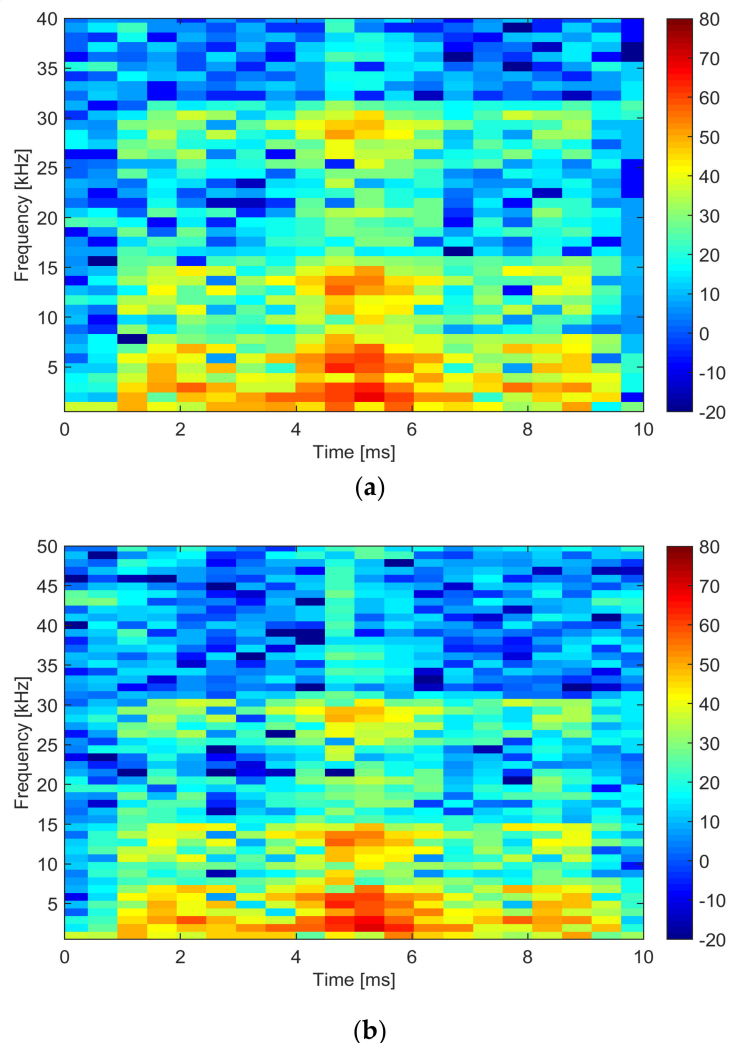
Figure 6. (**a**) Zoom on the frequency axis of Figure 5b for the frequency resolution of 976 Hz, where the change of the instantaneous frequency between 4 and 6 ms is well visible; and (**b**) additional spectrum obtained by replacing *symlet1* with *bior1.3*.

The compactness in time and frequency was evaluated considering two wavelets extensively used for PQ studies, the *db15* (equivalent to the *db20*) and the *sym8*. The results shown in Figure 7 (for the SMPS type Black at 90% of the rated power) reveal that *sym8* has some spectral leakage at the occurrence of the two peaks of the signal, at 1 ms and 4.5 ms; *db15* instead shows a limited increase of some scattered components without any visible burst of spectral leakage. Regarding the low frequency components, *db15* also shows a more coherent behavior where the second frequency bin keeps the lead

for 2 ms giving yield then to fourth bin, with a return around 4 ms. Behavior of *sym8* instead is more chaotic with no definite bin prevailing for at least some ms.

(**a**)

(**b**)
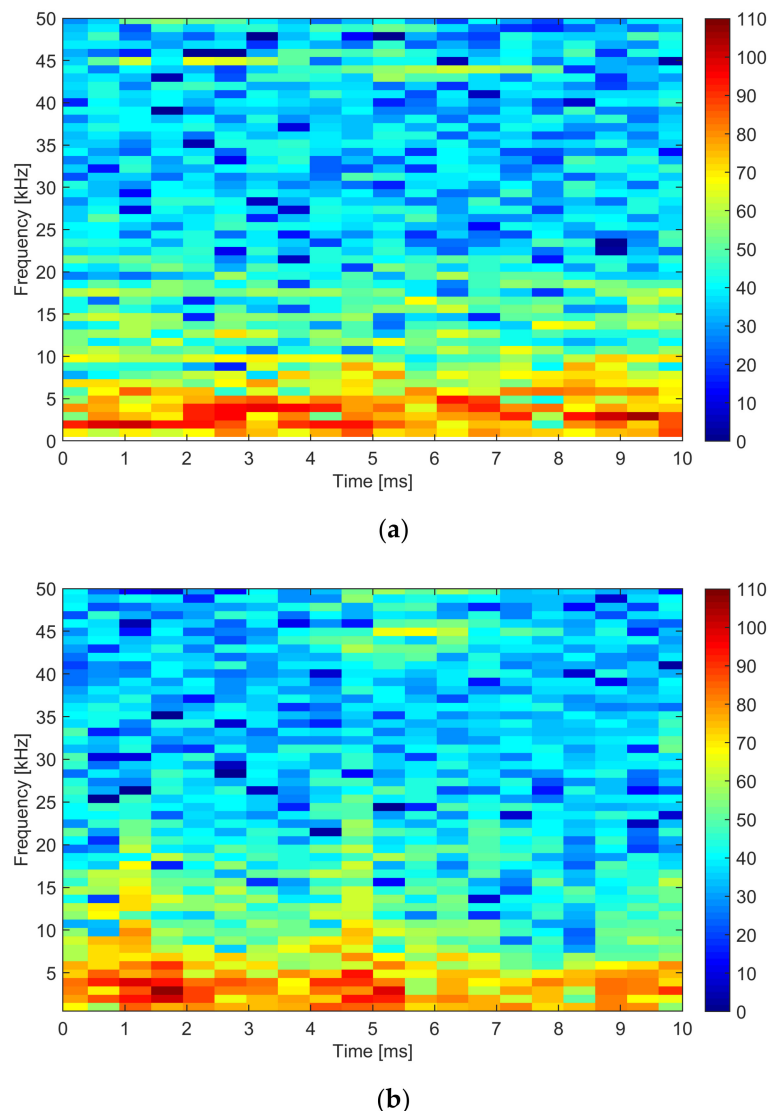
Figure 7. Comparison of two different wavelets in relation to localization on the time axis and spread to adjacent frequency bins; frequency resolution Δf = 976 Hz, number of levels L = 9: (**a**) *db15*; and (**b**) *sym8*. SMPS type Black at 90% of rated power.

As observed for the EEMD in Section 3.3, the best amplitude accuracy is reached for the faster components (those at about 44 and 88 kHz) that have better localization in both time and frequency: in this case, agreement for different frequency and time resolutions is within 0.6 dB for the results shown in Figure 5 (confirmed by some other tests done on different SMPSs). For nonstationary low-frequency components, the reference measurements themselves for assessment of accuracy are deemed by variability and uncertainty caused by the very nature of the signals.

3.2.2. Amplitude Accuracy and Spectrum Representation of WPT

The WPT behavior for the SMPS with constant switching frequency (named "Black" SMPS in the following) is analyzed showing the elements that concur to determine the amplitude accuracy.

As introduced in Section 2.3, the WPT spectra built with wpspectrum( ) is artificially adjusted so that the local intensity of each tile can be evaluated standalone. The adjustment consists in the

multiplication by the square root of the number *a* of tiles in the time direction (*a* = 20 in the present case) that is re-absorbed when aggregating in the rms sense all such tiles for each frequency bin to recover its rms, which for single tone calibration signals corresponds to the rms amplitude of the test signal itself.

The results of a comparison with STFT with 1 kHz frequency resolution and calculated using the Flat Top window are shown in Figure 8.

(**a**)

(**b**)
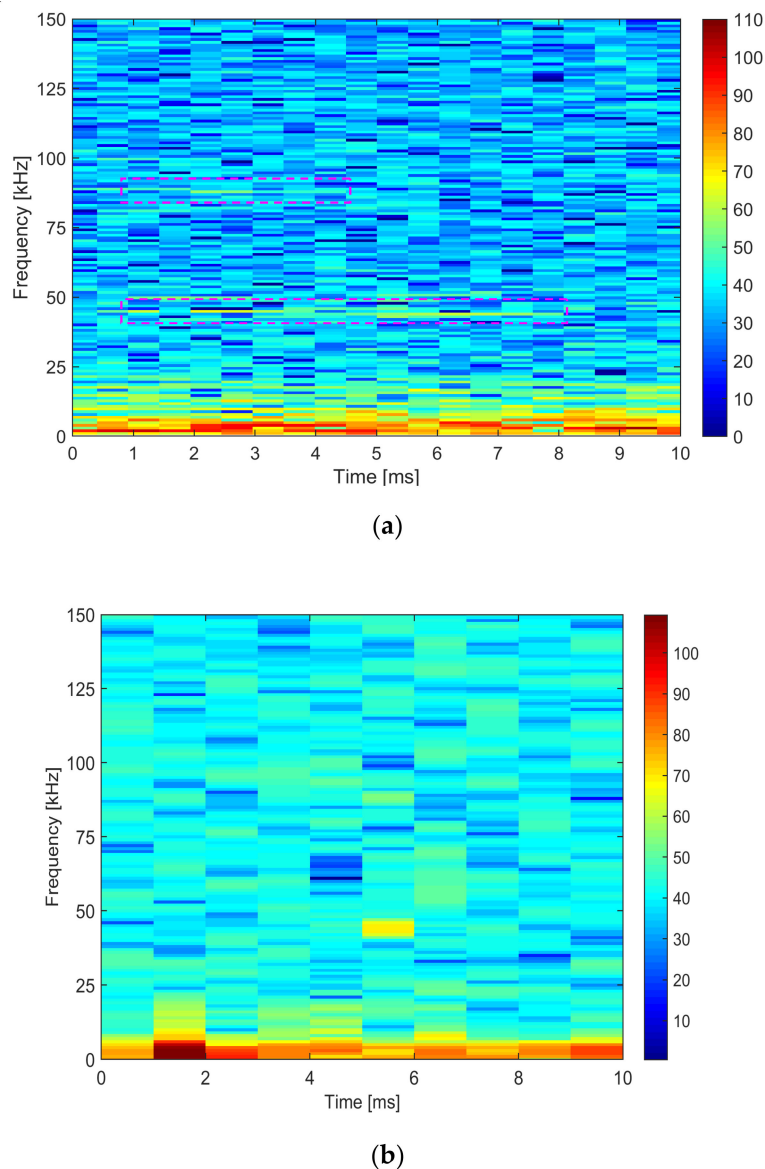
Figure 8. Black SMPS tested at 90% of rated power: (**a**) WPT spectrum obtained with *db15*, *L* = 9, Δf = 976 Hz; and (**b**) STFT spectrum with Δf = 1 kHz and time step Δt = 1 ms.

The two areas encircled by the pink rectangles are those of the 44 kHz and 88 kHz components, for which the WPT provides a thorough tracking (see Figure 8a), better than that appearing in the STFT spectrum (Figure 8b). The comparison between WPT spectrum and STFT shown in Figure 8 reveals that:

- WPT frequency resolution is superior, in terms of spectrum details and reduced leakage, which instead affect the STFT results (see, for instance, the central portion of the spectrum between 4 ms and 6 ms and the dynamic range of more than 30 dB for the background components (blue to light blue color)).
- The time resolution is also superior with the ability of tracking more closely signal dynamics.

- Regarding amplitude accuracy, we must distinguish between: (i) For narrowband switching components visible at 44 kHz and 88 kHz, there is a general agreement among WPT, STFT and the EMI receiver scan in frequency domain. We must observe that the receiver scan was made for a time interval much longer than the one covered by WPT and STFT, so that using max hold slightly larger values may be expected. (ii) The low frequency components are a byproduct of the switching pulses and evidently the instantaneous frequency is slightly variable, as result of non-linearity during oscillations. WPT confirms good tracking of such components and averaged values over adjacent bins are quite stable with respect to different frequency resolutions Δf.

Table 1 reports the results of the assessment of the amplitude accuracy for the three most prominent frequency bins shown in the first column. Reported values are the maxima, in line with the use of Flat Top for the STFT and max hold for the EMI receiver.

Table 1. Comparison of amplitudes of main spectrum components calculated with WPT and STFT and measured with EMI receiver (using the 1 kHz RBW results in Figure 4).

Frequency (kHz)	EMI Rec. (dBµV)	WPT (dBµV)	STFT (dBµV)
2–5	93.0	93.75–105.5 [1]	82.73–106.7 [1]
44	70.5	68.07, 71.51 [2]	69.04
88	57.5	60.60 [3]	53.27

[1] Range of maxima in the 2–4 kHz bins over 10 ms for 90% of bins; implicit averaging in this case is extremely important and WPT has the best resolution and the least averaging. [2] Five bins between 60.64 dBµV and 65.87 dBµV; with rms summation of adjacent bins carried out to cope with the 1 ms time resolution of the STFT, the results are 71.51 dBµV and 68.07 dBµV centered at 2.5 ms and 6.5 ms. [3] Two bins with 55.27 dBµV and 53.83 dBµV; with rms summation of adjacent bins carried out to cope with the 1 ms time resolution of the STFT, the result is 60.60 dBµV centered at 2.5 ms.

3.3. EMD and EEMD Performance

The EMD and EEMD were used in the R interface implementation Rlibeemd [30,31]. The measured voltage is analyzed first using EMD. As the boundaries of the signal may affect the decomposition of EMD-based algorithms [32], to avoid boundary problems, particular care was taken in the choice of an appropriate time record of 10 ms. Figure 9 shows the 12 IMFs extracted from the original signal. As demonstrated in [33], the EMD performs as a filter-bank sifting out the high-frequency harmonics first, whereas the low-frequency ones pass through the filter. IMFs 2 and 3 contain the information needed to represent the significant part of the frequency spectrum, i.e., the three peaks corresponding to the switching frequency (about 44 kHz) of the SMPS and its second and third harmonics. IMF 2 contains the information related to the second and third harmonics of the fundamental frequency, whereas IMF 3 contains the information of the switching frequency. Performing a FFT on the sum of these two IMFs yields the red spectrum in Figure 10, whereas the blue spectrum is the FFT of the original signal. A Flat Top window is applied to the original signal and IMFs in order to maximize the amplitude estimate [15].

As shown in Figure 10, the three peaks are predicted with good accuracy, although there is a difference of about 1 dB with the FFT of the original signal for the peak at the fundamental frequency. Considering these two IMFs 2 and 3 only has the effect of filtering the low-frequency content of the measured voltage, which is collected in IMFs 4–13. IMFs 4 and 5 contain the information related to the 100 Hz ripple components (whose period corresponds to 10 ms, as shown in Figure 2). These IMFs are those with the largest amplitude and represent the low-frequency part of the signal in the frequency domain. IMFs 2–5 thus contain sufficient information to represent the signal, as shown in Figure 11. As can be seen, this spectrum slightly differs from the spectrum of the original signal up to 150 kHz. The fundamental, second and third harmonics are predicted with good accuracy with respect to the FFT of the original signal. Some information on the fundamental frequency may then be contained in IMFs 4 and 5 due to mode mixing, as mentioned in Section 2.4. Of course, the upper part of the frequency range is not predicted accurately, as the lowest order IMF (that containing the information on

higher frequencies) has not been considered. Nevertheless, the supraharmonics spectrum 2–150 kHz is well represented with just four IMFs obtained with EMD.
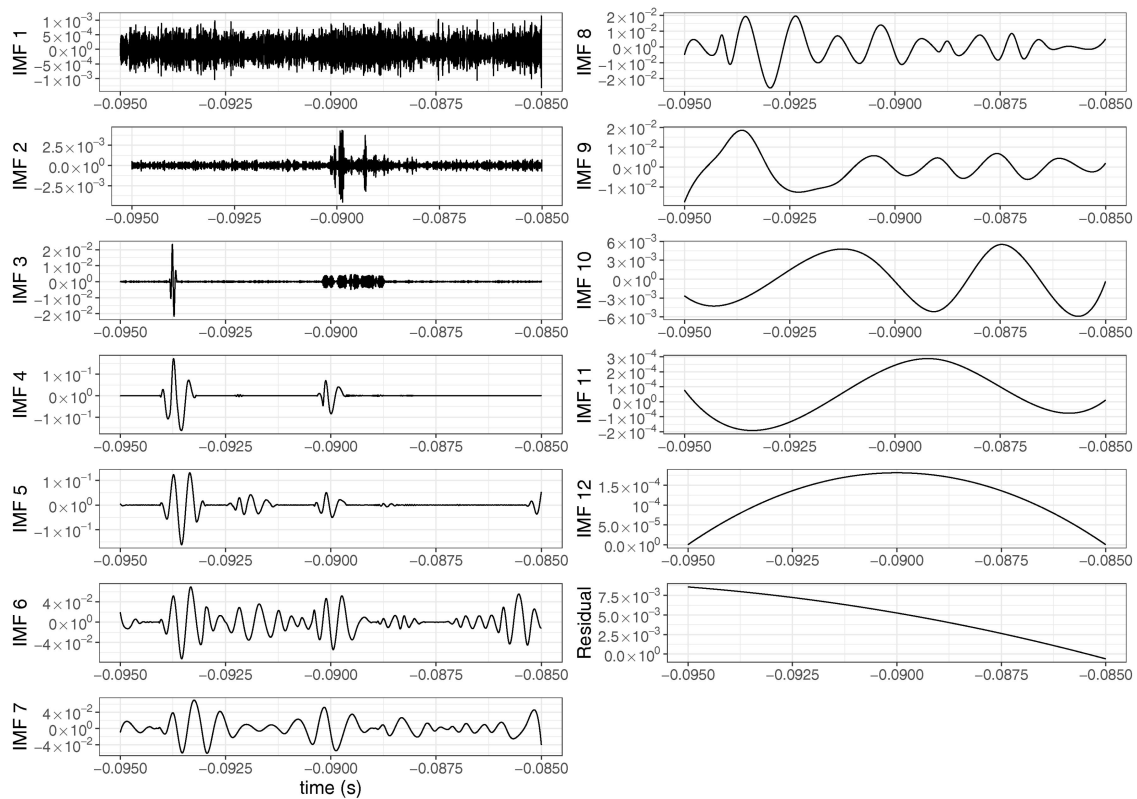
Figure 9. IMFs extracted with the EMD procedure.
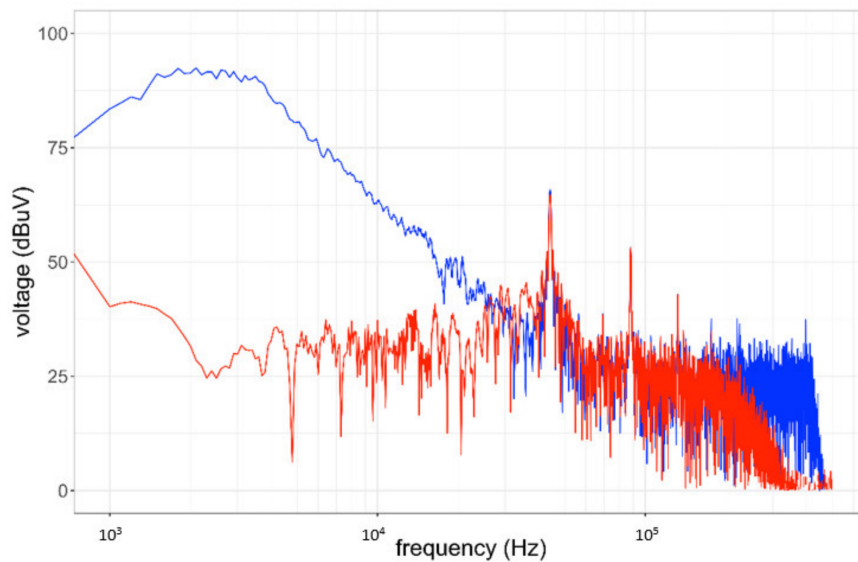
Figure 10. Comparison of the FFT spectra obtained from IMFs 2 and 3 extracted with EMD (**red**) and from the original signal (**blue**).

The application of the EEMD yields the same number of IMFs as EMD, 12, as shown in Figure 12. The information related to the 100 Hz ripple components is contained in IMFs 5–9, being IMFs 6 and 7 those with the largest amplitude. To represent the signal in the frequency domain, only IMFs 2–7 are needed. The high-frequency information of the signal is now distributed over three IMFs (IMFs 2–4), as shown in Figure 13. The accuracy with which the first two peaks are determined is very

good; however, although the amplitude of the third harmonic of the fundamental is predicted quite accurately, the noise floor beyond 100 kHz raises making it less clearly visible than in the case of the EMD. The filtering effect on the low-frequency components of the spectrum is still evident. By adding IMFs 5–7 and performing the FFT on the sum of these six IMFs, the red spectrum of Figure 14 is obtained, which is in fairly good agreement with that of the original signal.

By means of the application of FFT to the relevant modal components obtained with EMD, it is shown that the frequency extraction ability of the EMD is consistent and strong [34].

The results of comparison with STFT with 1 kHz frequency resolution, a 1 ms time step and a Flat Top window are shown in Figures 15 and 16. The former figure refers to the application of STFT to the signal obtained composing IMFs 2 and 3 extracted with EMD; the latter to the application of STFT to the signal obtained composing IMFs 2–4 extracted with EEMD. The amplitudes are the maximum values obtained by the successive FFTs that compose the STFT, as it would be with a spectrum analyzer set to max hold. It can be noticed that the amplitudes of the first peak (at 44 kHz, with 68.27 dBμV and 69.97 dBμV, respectively) and of the second peak (at 88 kHz, with 57.59 dBμV and 58.51 dBμV, respectively) are in agreement with those shown in Table 1 for WPT and EMI receiver data, thus confirming the suitability of the approach in the analysis of EMI.
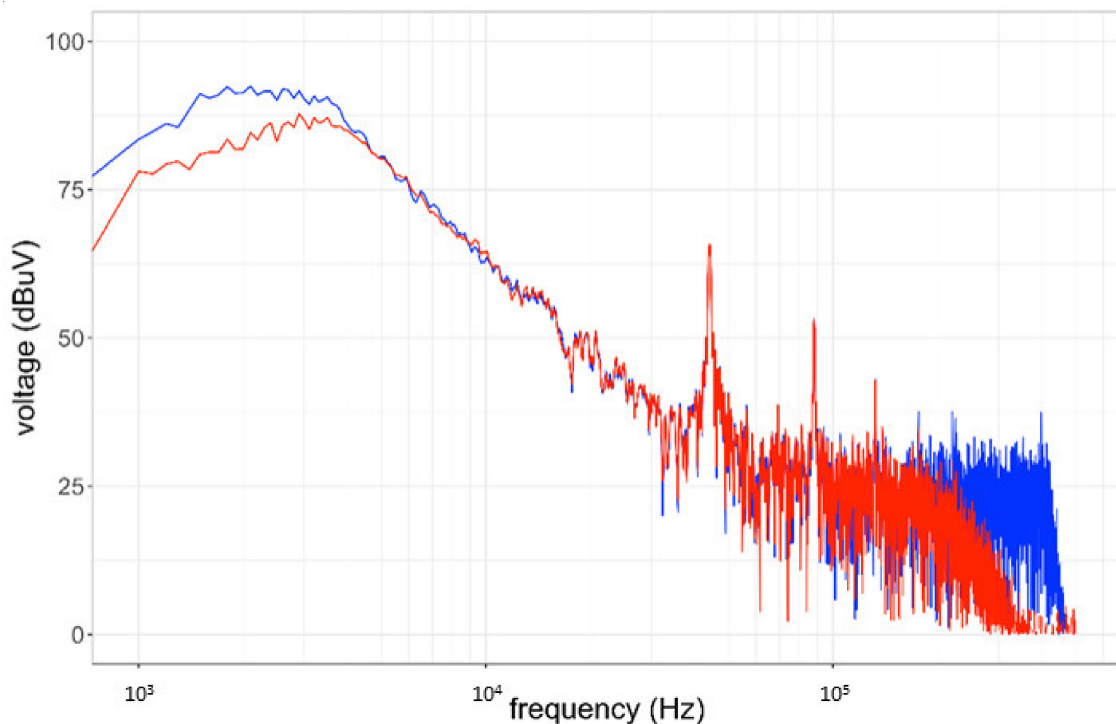
Figure 11. Comparison of the FFT spectra obtained from IMFs 2–5 extracted with EMD (**red**) and from the original signal (**blue**).
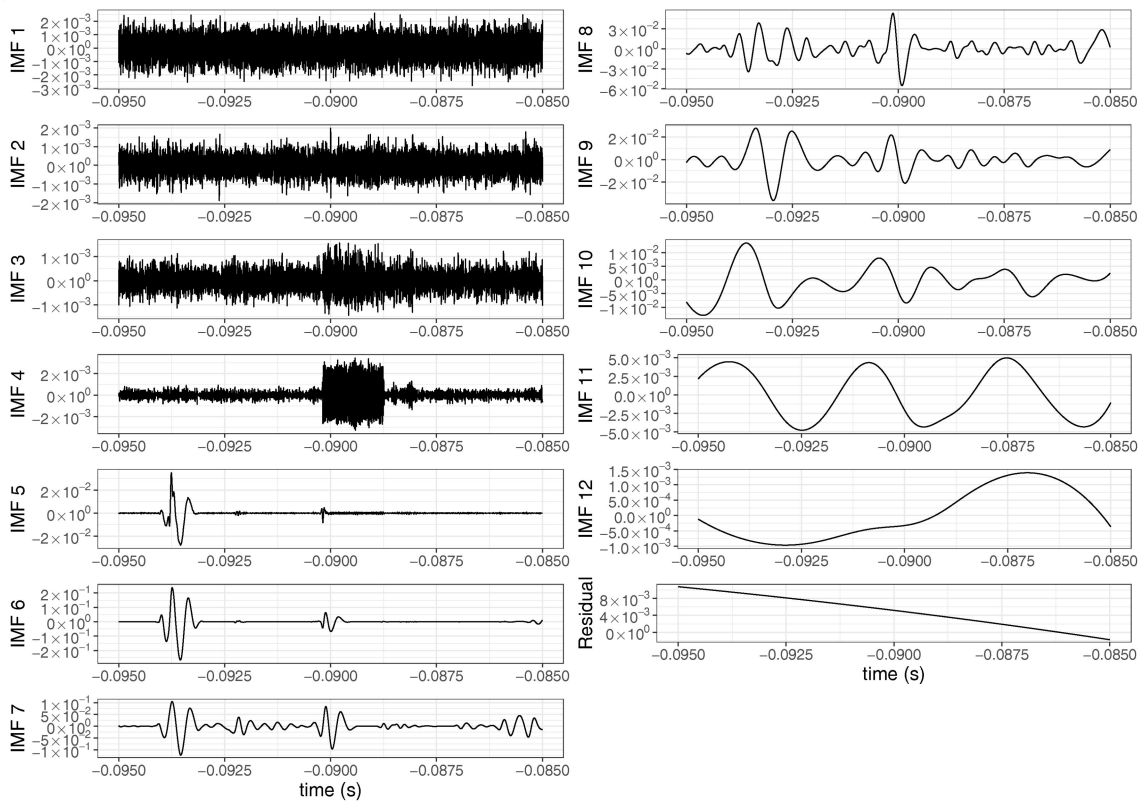
Figure 12. IMFs extracted with the EEMD procedure.
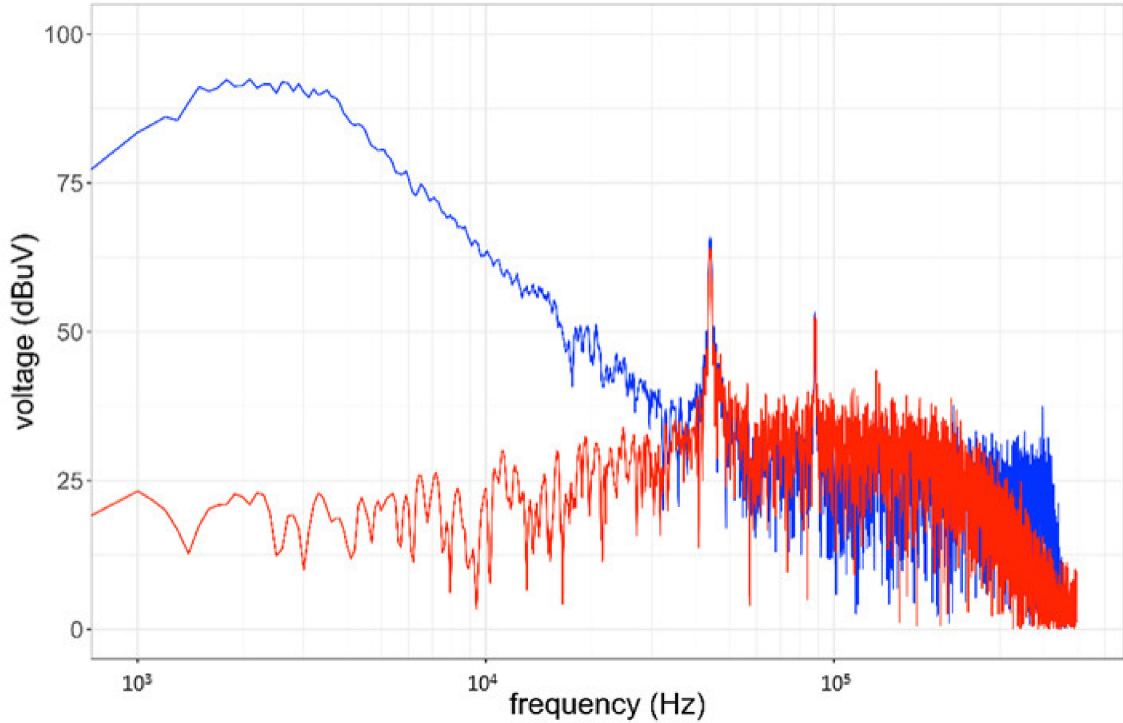
Figure 13. Comparison of the FFT spectra obtained from IMFs 2–4 extracted with EEMD (**red**) and from the original signal (**blue**).
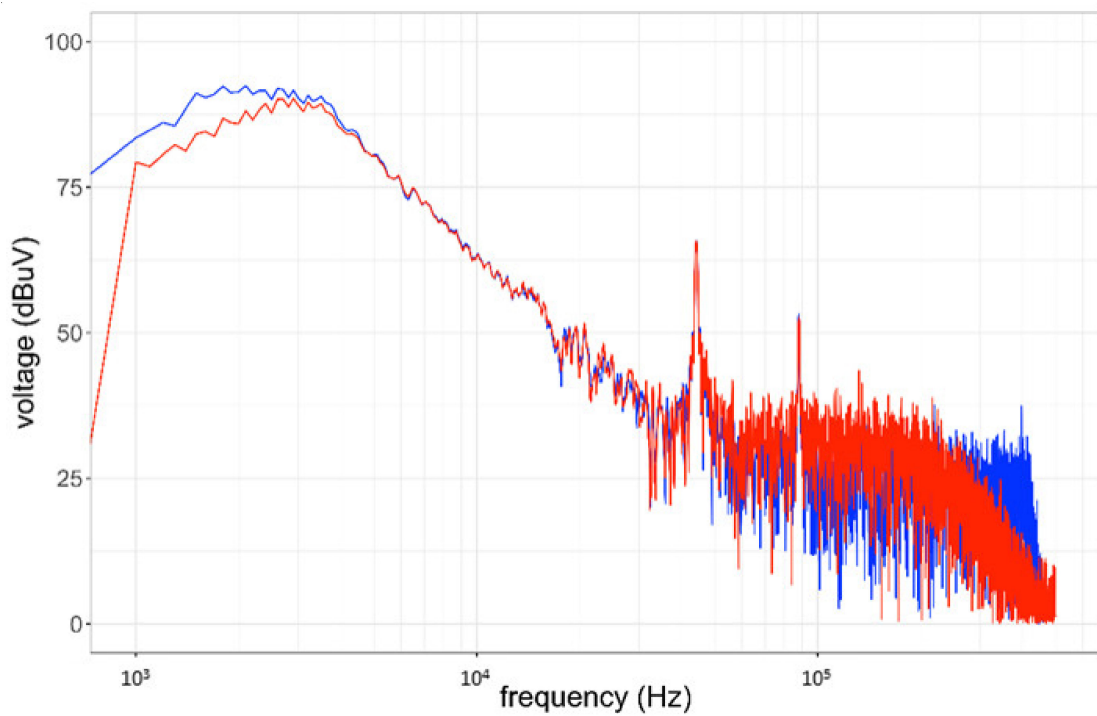
Figure 14. Comparison of the FFT spectra obtained from IMFs 2–7 extracted with EEMD (**red**) and from the original signal (**blue**).
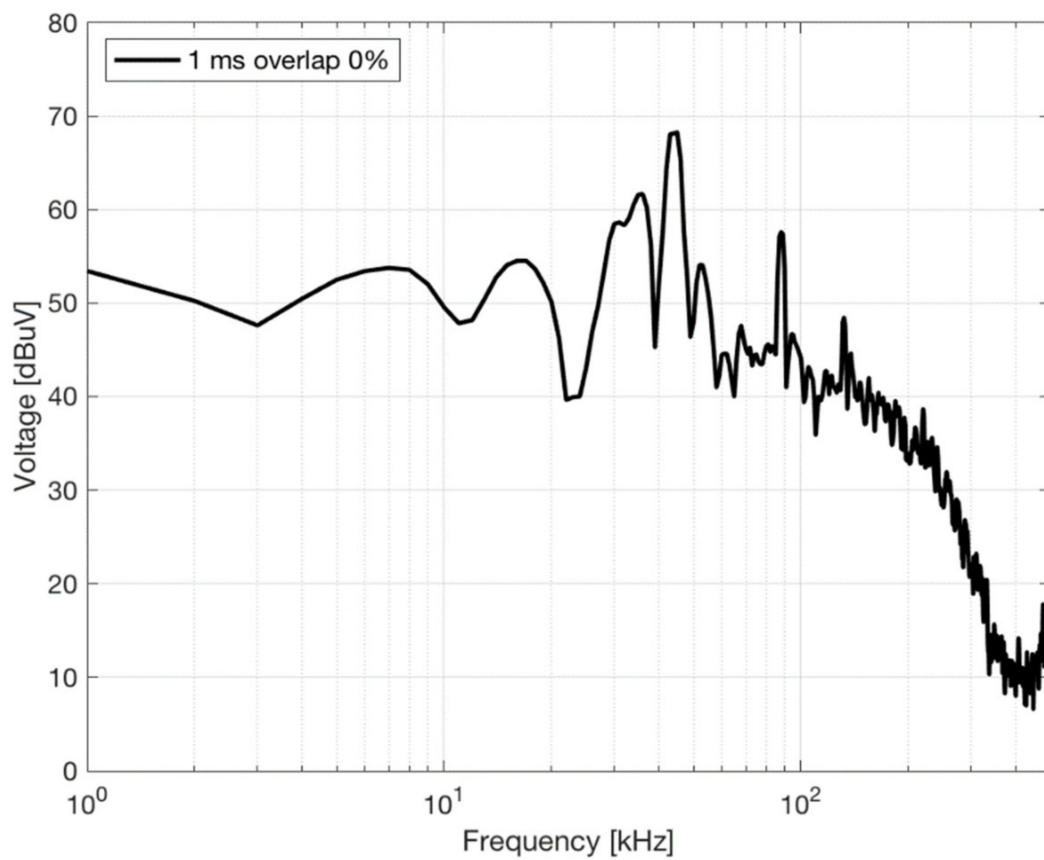
Figure 15. STFT spectrum with Δf = 1 kHz and time step Δt = 1 ms of the signal resulting from the composition of IMFs 2 and 3 extracted with EMD.
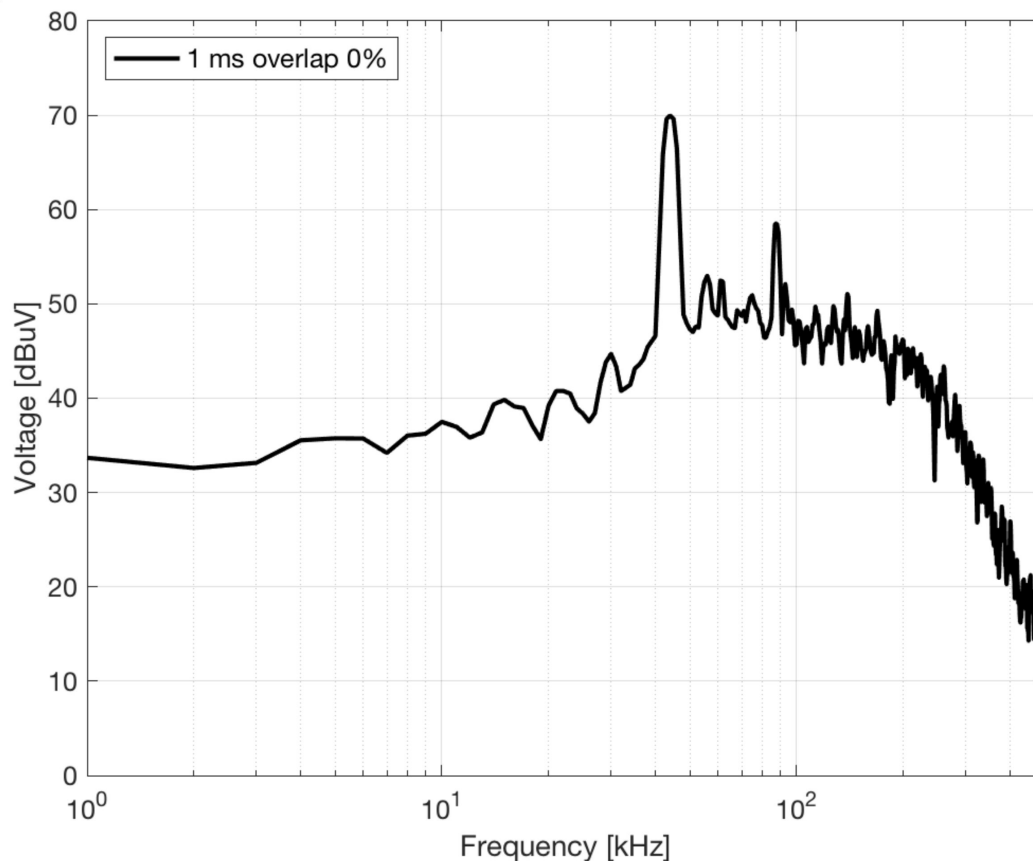
Figure 16. STFT spectrum with $\Delta f = 1$ kHz and time step $\Delta t = 1$ ms of the signal resulting from the composition of IMFs 2 to 4 extracted with EEMD.

4. Conclusions

The problem of the assessment of conducted emissions of Switched Mode Power Supplies (SMPSs) using time-domain sampled data is considered. Emissions measured with a Digital Sampling Oscilloscope using a Line Impedance Stabilization Network are characterized by fast switching pulses and damped oscillations, posing a problem for reconciling amplitude accuracy, suitable frequency resolution and fast time response to track signal dynamics.

Suitable processing techniques are discussed, contrasted to the most popular approach of using Discrete Fourier Transform analysis. The DFT drawbacks are pointed out in Section 2, in relation to the unfavorable time support and frequency resolution, as well as to the known issues of amplitude accuracy and spectral leakage. Two techniques (Wavelet Packet Transform (WPT) and Empirical Mode Decomposition (EMD)) based on different principles are then evaluated, with the objective of an adequate and accurate handling of signal characteristics, as reflected in its spectral components and their amplitude, for the assessment of SMPS conducted emissions.

WPT and EMD are compared for complexity, ease of implementation and, most of all, usability of the output and suitability to identify and represent the relevant spectral components. The objective is that of an accurate amplitude estimate and assessment of hypothetical compliance to limits of emissions. The output representation of the WPT is more effective, in that the data are represented as one might expect for not only comparison with limits, but also analysis of short-term disturbance (e.g., for victim circuits characterized by some transient susceptibility) and in general tracking and troubleshooting of byproducts along the evolution of the signal.

WPT shows a general consistency and robustness with respect to the change of the number of levels L and downsampling q (applied to the original 10 MSa/s sample rate). Similarly, the change of mother wavelet is verified, passing in one case from the *symlet* (linear phase and asymmetric)

to the *biorthogonal* (linear phase and symmetric), using for each the minimum order, and in a second case using db15 ad sym8, observing a larger spectrum leakage for the latter. The sensitivity analysis indicates a variability of less than 1 dB when comparing values averaged with the adjacent time and frequency bins; maximum observed difference for the peak values is 3.6 dB for the broad 2.2 kHz component that suffers the largest variability.

The application of EMD and EEMD algorithms yields a limited number of IMFs that are sufficient to represent the original signal fairly accurately (four and six, respectively). Moreover, the representation can be made even more compact by exploiting the filtering effect of the IMFs on the low-frequency components of the signal, thus reducing the number of IMFs necessary to represent the most significant part of the spectrum to two and three, respectively. EMD represents the spectrum for frequencies larger than 100 kHz better than EEMD, which seems to produce a higher noise floor.

Future work will be focused on the identification of quantitative indices of performance and a framework to evaluate systematically the performances of the various implementations, especially for the WPT, where the number of mother wavelets and filter implementations is almost uncountable.

References

1. Thomas, D. Conducted emissions in distribution systems (1 kHz–1 MHz). *IEEE Electromagn. Compat. Mag.* **2013**, 2, 101–104. [CrossRef]
2. Larsson, E.A.; Bollen, M.H.; Wahlberg, M.G.; Lundmark, C.M.; Ronnberg, S.K. Measurements of high-frequency (2–150 kHz) distortion in low-voltage networks. *IEEE Trans. Power Deliv.* **2010**, 25, 1749–1757. [CrossRef]
3. Frey, D.; Schanen, J.; Quintana, S.; Bollen, M.; Conrath, C. Study of high frequency harmonics propagation in industrial networks. In Proceedings of the EMC Europe, Rome, Italy, 17–21 September 2012.
4. Bartak, G.F.; Abart, A. EMI in the frequency range 2 kHz–150 kHz. In Proceedings of the 22nd International Conference and Exhibition on Electricity Distribution (CIRED 2013), Stockholm, Sweden, 10–13 June 2013.
5. Klatt, M.; Meyer, J.; Schegner, P. Comparison of measurement methods for the frequency range of 2 kHz to 150 kHz. In Proceedings of the 2014 16th International Conference on Harmonics and Quality of Power (ICHQP), Bucharest, Romania, 25–28 May 2014.
6. Sandrolini, L.; Thomas, D.W.P.; Sumner, M.; Rose, C. Measurement and Evaluation of the Conducted Emissions of a DC/DC Power Converter in the Frequency Range 2–150 kHz. In Proceedings of the 2018 IEEE Symposium on Electromagnetic Compatibility, Signal Integrity and Power Integrity (EMC, SI & PI), Long Beach, CA, USA, 30 July–3 August 2018.
7. Sandrolini, L.; Mariscotti, A. Techniques for the Analysis of Time-Domain Conducted Emissions of SMPS in Smart Grids. In Proceedings of the 2019 IEEE International Conference on Environment and Electrical Engineering and 2019 IEEE Industrial and Commercial Power Systems Europe, Genova, Italy, 11–14 June 2019.
8. Ensini, L.; Sandrolini, L.; Thomas DW, P.; Sumner, M.; Rose, C. Conducted Emissions on DC Power Grids. In Proceedings of the International Symposium on Electromagnetic Compatibility (EMC EUROPE), Amsterdam, The Netherlands, 27–30 August 2018.
9. Sandrolini, L.; Pasini, G. Study of the Conducted Emissions of an SMPS Power Converter from 2 to 150 kHz. In Proceedings of the IEEE International Conference on Environment and Electrical Engineering and 2018 IEEE Industrial and Commercial Power Systems Europe, Palermo, Italy, 12–15 June 2018.
10. CENELEC EN 61000-4-19. *Electromagnetic Compatibility (EMC)—Part 4–19: Testing and Measurement Techniques—Test for Immunity to Conducted, Differential Mode Disturbances and Signalling in the Frequency Range 2 kHz to 150 kHz at a.c. Power Ports*; European Committee for Electrotechnical Standardization: Brussels, Belgium, 2014.

11. CENELEC EN 55014-1. *Electromagnetic Compatibility—Requirements for House—Hold Appliances, Electric Tools and Similar Apparatus—Part 1: Emission*; European Committee for Electrotechnical Standardization: Brussels, Belgium, 2017.

12. CENELEC EN 55015. *Limits and Methods of Measurement of Radio Disturbance Characteristics of Electrical Lighting and Similar Equipment*; European Committee for Electrotechnical Standardization: Brussels, Belgium, 2014.

13. CENELEC EN 61000-4-30. *Electromagnetic Compatibility—Part 4–30: Testing and Measurement Techniques—Power Quality Measurement Methods*; European Committee for Electrotechnical Standardization: Brussels, Belgium, 2015.

14. CENELEC EN 50065-1. *Signalling on Low-Voltage Electrical Installations in the Frequency Range 3 kHz to 148.5 kHz—Part 1: General Requirements, Frequency Bands and Electromagnetic Disturbances*; European Committee for Electrotechnical Standardization: Brussels, Belgium, 2012.

15. Sandrolini, L.; Mariscotti, A. Impact of Short-Time Fourier Transform Parameters on the Accuracy of EMI Spectra Estimates in the 2–150 kHz Supraharmonics Interval. *Electr. Power Syst. Res..* under review.

16. Barros, J.; Diego, R.I. Analysis of Harmonics in Power Systems Using the Wavelet-Packet Transform. *IEEE Trans. Instrum. Meas.* **2008**, *57*, 63–69. [CrossRef]

17. Masoum, M.A.S.; Jamali, S.; Ghaffarzadeh, N. Detection and classification of power quality disturbances using discrete wavelet transform and wavelet networks. *IET Sci. Meas. Technol.* **2010**, *4*, 193–205. [CrossRef]

18. Lodetti, S.; Bruna, J.; Melero, J.J.; Sanz, J.F. Wavelet Packet Decomposition for IEC Compliant Assessment of Harmonics under Stationary and Fluctuating Conditions. *Energies* **2019**, *12*, 4389. [CrossRef]

19. Zhu, S.-X.; Liu, H. Simulation study of power harmonic based on Daubechies wavelet. In Proceedings of the 2010 International Conference on E-Product E-Service and E-Entertainment, Henan, China, 7–9 November 2010.

20. Mariscotti, A. Characterization of Power Quality transient phenomena of DC railway traction supply. *Acta Imeko* **2012**, *1*, 26–35. [CrossRef]

21. Mariscotti, A. Methods for Ripple Index evaluation in DC Low Voltage Distribution Networks. In Proceedings of the IEEE Instrumentation and Measurement Technical Conference (IMTC), Warsaw, Poland, 2–4 May 2007.

22. Hai, Y.; Chen, J.-Y. RMS and power measurements based on wavelet packet decomposition using special IIR filter bank. In Proceedings of the 2011 International Conference on Electronic & Mechanical Engineering and Information Technology, Harbin, China, 12–14 August 2011.

23. Huang, N.E.; Wu, Z. A review on Hilbert-Huang transform: Method and its applications to geophysical studies. *Rev. Geophys.* **2008**, *46*, 1–23. [CrossRef]

24. Li, H.; Zhang, Y.; Zheng, H. Hilbert-Huang transform and marginal spectrum for detection and diagnosis of localized defects in roller bearings. *J. Mech. Sci. Technol.* **2009**, *23*, 291–301. [CrossRef]

25. Fu, K.; Qu, J.; Chai, Y.; Zou, T. Hilbert marginal spectrum analysis for automatic seizure detection in EEG signals. *Biomed. Signal Proc. Control* **2015**, *18*, 179–185. [CrossRef]

26. Zhaohua, W.; Huang, N.E. Ensemble Empirical Mode Decomposition: A Noise-Assisted Data Analysis Method. *Adv. Adapt. Data Anal.* **2009**, *1*, 1–41.

27. Gong, X.; Ferreira, J.A. Comparison and Reduction of Conducted EMI in SiC JFET and Si IGBT-Based Motor Drives. *IEEE Trans. Power Electron.* **2014**, *29*, 1757–1767. [CrossRef]

28. Mariscotti, A. Normative Framework for the Assessment of the Radiated Electromagnetic Emissions from Traction Power Supply and Rolling Stock. In Proceedings of the 2019 IEEE Vehicle Power and Propulsion Conference (VPPC), Hanoi, Vietnam, 14–17 October 2019.

29. IEC 61000-4-7. *Electromagnetic Compatibility (EMC)—Part 4–7: Testing and Measurement Techniques—General Guide on Harmonics and Interharmonics Measurements and Instrumentation, for Power Supply Systems and Equipment Connected Thereto*; International Electrotechnical Commission: Geneva, Switzerland, 2009.

30. Helske, J.; Luukko, P.J. Rlibeemd: Ensemble Empirical Mode Decomposition (EEMD) and Its Complete Variant (CEEMDAN); R Package Version 1.4.1. 2018. Available online: https://github.com/helske/Rlibeemd (accessed on 1 October 2020).

31. Luukko, P.J.; Helske, J.; Räsänen, E. Introducing libeemd: A program package for performing the ensemble empirical mode decomposition. *Comput. Stat.* **2006**, *31*, 545–557. [CrossRef]

32. Stallone, A.; Cicone, A.; Materassi, M. New insights and best practices for the successful use of Empirical Mode Decomposition, Iterative Filtering and derived algorithms. *Sci. Rep.* **2020**, *10*, 15161. [CrossRef] [PubMed]

33. Feldman, M. Analytical basics of the EMD: Two harmonics decomposition. *Mech. Syst. Signal Process.* **2009**, *23*, 2059–2071. [CrossRef]
34. Ge, H.; Chen, G.; Yu, H.; Chen, H.; An, F. Theoretical Analysis of Empirical Mode Decomposition. *Symmetry* **2018**, *10*, 623. [CrossRef]

Publisher's Note: MDPI stays neutral with regard to jurisdictional claims in published maps and institutional affiliations.